The disengaging brain: Dynamic transitions from cognitive engagement and alcoholism risk

Enrico Amico [a,b], Mario Dzemidzic [c], Brandon G. Oberlin [c,d], Claire R. Carron [c], Jaroslaw Harezlak [e], Joaquín Goñi [a,b,f,*,1], David A. Kareken [c,1,**]

[a] Purdue Institute for Integrative Neuroscience, Purdue University, USA
[b] School of Industrial Engineering, Purdue University, USA
[c] Department of Neurology, Indiana University School of Medicine, Indiana Alcohol Research Center, USA
[d] Department of Psychiatry, Indiana University School of Medicine, USA
[e] Department of Epidemiology and Biostatistics, Indiana University, USA
[f] Weldon School of Biomedical Engineering, Purdue University, USA

ABSTRACT

Human functional brain connectivity is usually measured either at "rest" or during cognitive tasks, ignoring life's moments of mental transition. We propose a different approach to understanding brain network transitions. We applied a novel independent component analysis of functional connectivity during motor inhibition (stop signal task) and during the continuous transition to an immediately ensuing rest. A functional network reconfiguration process emerged that: (i) was most prominent in those *without* familial alcoholism risk, (ii) encompassed brain areas engaged by the task, yet (iii) appeared only transiently after task cessation. The pattern was not present in a pre-task rest scan or in the remaining minutes of post-task rest. Finally, this transient network reconfiguration related to a key behavioral trait of addiction risk: reward delay discounting. These novel findings illustrate how dynamic brain functional reconfiguration during normally unstudied periods of cognitive transition might reflect addiction vulnerability, and potentially other forms of brain dysfunction.

1. Introduction

Functional organization of the human brain is usually assessed either at "rest" (quiet introspection without external task demands) or during tasks requiring goal-directed behavior (Gonzalez-Castillo and Bandettini, 2018). Yet a rigid distinction between rest and directed mental effort fails to capture the critical periods of mental state transitions that characterize the cognitive demands of daily life. Rather, everyday life demands frequent transitions between introspection, when the brain's default mode network (DMN) activity is prominent (Raichle et al., 2001; Shulman et al., 1997), and goal-directed behaviors supported by "task positive" networks (Cole et al., 2014; Shine et al., 2017).

At odds with a simplistic rest-task dichotomy is the presence of task-like connectivity within periods of rest (Chen et al., 2018). "Resting" connectivity is also different in the immediate wake of mental effort when compared to rest after a longer period of time (Amico et al., 2019; Chen et al., 2018; Lewis et al., 2009; Pyka et al., 2009). As opposed to a simple binary switch from active to resting brain, a sequence of network functional reconfigurations is likely needed *en route* to rest (Shine et al.,

2017). Moreover, the nature of dynamic brain reconfiguration appears central to higher-order thinking, as better cognitive performance is associated with small, efficient updates in brain connectivity across states of rest and task engagement (Schultz and Cole, 2016). By extension, such dynamic network reconfigurations would also seem a plausible marker of psychiatric disease liability. This creates a need for new ways of examining brain network functional reconfiguration in humans.

Here we investigated how brain state transitions and their associated functional connectomes relate to a family history of alcoholism (FHA). FHA is not only one of the strongest predictors of developing an alcohol use disorder, but it is also a risk factor for other behavioral disorders (Heiman et al., 2008; Moss et al., 2007; Nurnberger et al., 2004b; Walters et al., 2018). Executive brain areas seem a prime target of study, as evidence indicates that executive control of behavior is both heritable and impaired in the offspring of alcoholic parents (Dougherty et al., 2015; Gustavson et al., 2017; Nigg et al., 2004; Young et al., 2009). Similarly, the frontal brain anatomy and function that undergird executive behaviors have been shown to be affected by FHA and predict binge drinking (Cservenka, 2016; Hardee et al., 2014; Porjesz et al., 2005; Whelan et al., 2014).

An important aspect of executive function involves efficient changes in connectivity between mental states (Braun et al., 2015; Gallen et al., 2016; Schultz and Cole, 2016; Shine et al., 2019). Furthermore, Acheson et al. (2014) showed that, in a Go/No-Go motor inhibition paradigm, those with FHA had greater blood oxygenation level dependent (BOLD) activity during both blocks of mixed Go and No-Go (inhibitory) stimuli, as well as blocks of Go stimuli alone (each block compared to baseline). As commented upon by (Colrain, 2015), several of these regions of greater BOLD activity in the FHA group comprised nodes in the default mode network (DMN). Although the Acheson et al. study involved directed cognitive effort, the DMN is a network that is most prominent at "rest" (Raichle et al., 2001; Shulman et al., 1997). While other explanations for the Acheson et al. findings are possible, they could arise if those with FHA deactivate less between trials (i.e., during brief periods of lower response demands). In the context of data indicating that task-induced BOLD activation magnitude relates to resting connectivity strength (Mennes et al., 2010), these collective observations led us to hypothesize that FHA might involve altered connectivity patterns or reconfiguration processes when transitioning between mental states of high and low cognitive demand.

We therefore designed a study in which we could test for FHA-related connectivity differences during the transition from active behavioral engagement (motor inhibition in the stop signal task; SST) to rest. We tested our hypothesis using a novel data-driven, connectivity-based independent component analysis (connICA (Amico et al., 2017)). The results of this analysis revealed a specific functional reconfiguration process that: (i) was associated with FHA, (ii) encompassed a number of brain areas actively engaged by the task, yet (iii) emerged during the subsequent rest period, (iv) and only transiently during an approximate 3 min period, 15–20 s after task cessation. Critically, (v) the reconfiguration was *not* present in a pre-task rest scan, or in the final four minutes of rest. Finally, a *post-hoc* analysis in a subset of subjects revealed associations between the prominence of this functional reconfiguration process and a key addiction-related trait behavioral risk: delay discounting of reward.

These novel findings provide a critical foundation for understanding how brain functional networks reconfigure in task transitions, and how this dynamic reorganization relates to potential markers of brain dysfunction.

2. Methods

2.1. Subject information

All subjects signed an informed consent prior to study procedures, all of which were approved by the Indiana University Institutional Review Board. Fifty four subjects (23 positive FHA, mean age = 23.0, SD = 1.6, 9 men; 31 negative FHA, mean age = 22.4, SD = 1.6, 16 men; Table 1) completed fMRI. Subjects were classified as FHA positive if they had at least one first degree relative with a history of alcoholism. Subjects were classified as FHA negative if they had no first or second degree relatives with any history of alcoholism. Family history was established by interviewing the subject using the family history module of the semi-structured assessment for the genetics of alcoholism (SSAGA; (Bucholz et al., 1994)). Three FHA positive subjects had affected mothers, but reported that their mothers did not drink during pregnancy. These three subjects had between two and four years of college education, had no obvious facial abnormalities as reported by the interviewing technicians, and had go and stop signal reaction times (see below) within one standard deviation of the remainder of the sample.

2.2. Stop signal task

The SST was programmed using E-Prime 2.0 software (Psychology Software Tools Inc., Sharpsburg, PA), and consisted of 54 Go trials and 26 Stop trials. Go trials required a left or right button press on an MRI-

Table 1
Subject characteristics (N = 54).

	FHA positive (n = 23, 9 men)		FHA negative (n = 31, 16 men)	
	Mean (SD)	Range	Mean (SD)	Range
Age	23.04 (±1.64)	21–26	22.35 (±1.58)	21–26
Education (years)	15.32 (±1.25)	13–18	15.23 (±1.20)	14–19
SSRT[a] (ms)	250 (±48)	157–397	230 (±52)	124–346
AUDIT[b]	10.26 (±6.52)[e]	2–29	7.26 (±3.92)	1–20
CESD[c]	8.04 (±5.52)[e]	1–24	4.57 (±4.21)	0–17
Drinks per week	12.27 (±11.46)[e]	1.80–51.40	7.12 (±4.91)	1.20–20.80
Alcohol Grams/ Week TBW[d]-normalized	3.59 (±2.77)[e]	0.79–11.77	2.25 (±1.66)	0.25–7.98

[a] Stop Signal Response Time; time to withdraw a response.
[b] Alcohol Use Disorders Identification Test.
[c] Center for Epidemiologic Studies Depression scale.
[d] Total Body Water.
[e] FHA significant difference, two-tailed *t*-test $p < 0.05$.

compatible button box (Current Designs, Philadelphia, PA) to horizontal blue arrows pointing left or right. Subjects were instructed to respond as quickly and as accurately as possible. Stop trials occurred immediately after a Go stimulus, and were signaled by a red up-pointing arrow, indicating the need to inhibit the Go response. An adaptive staircase algorithm adjusted the delay between Go and Stop stimuli in 50 ms increments to target a stop inhibition rate of 50%. Estimated stop signal response time (SSRT) was calculated by subtracting a subject's average stop-signal delay from that subject's *x*th percentile Go RT, where *x* corresponds to the stop failure rate (Band et al., 2003). Thus, if a subject failed to stop on 45% of stop trials, the Go RT subtracted from the average stop-signal delay would be that of the 45th percentile of the subject's Go RT distribution. A mirror on the head coil permitted subjects to view stimuli as back-projected on a screen at the rear of the scanner bore. Prior to imaging, subjects briefly practiced the task (8 Go and 7 Stop trials) on a laptop outside the imaging suite.

2.3. Delay discounting task

Prior to MRI, subjects also performed a delay discounting task on a laptop outside the scanner. The task was programmed using E-Prime 2.0 software (Psychology Software Tools Inc., Sharpsburg, PA), and consisted of 60 binary choice trials; 5 trials for each of the 6 delays, duplicated for $20 and $200 standard amounts. An adaptive staircase procedure adjusted the immediate amount (initially half the standard) down for immediate choices and up for delayed choices, converging on the subjective preference for immediate money across delays (Du et al., 2002). Delays were 2 days, 1 week, 1 month, 6 months, 1 year, and 5 years. Amount/delay combinations and the presentation side were pseudorandomized. The task was not implemented in the first four study subjects, while data for four additional subjects were excluded for nonsystematic discounting of >25% deviation (based on (Johnson and Bickel, 2008)), resulting in a sample of *n* = 46. There were no significant group differences in the demographics reported in Table 1 between the *n* = 8 subjects left out and the n = 46 sample with available delay discounting data.

2.4. MRI acquisition

Subjects were imaged on a 3T Siemens Prisma MRI scanner with a 64-channel head coil, and with neck elements turned off. For both (rest and task-rest) functional MRI scans, we employed a multi-band (MB) blood oxygenation level dependent (BOLD) contrast sensitive sequence as

detailed in Xu et al., (2013): gradient-echo echo-planar imaging (GE-EPI), MB slice acceleration factor 3, repetition/echo time TR/TE = 1, 200 ms/29 ms, flip angle 65°, 2.5 × 2.5 × 2.5 mm³ voxels, 220 mm × 220 mm field of view, 54 interleaved axial slices. Two BOLD fMRI scans were performed: 1) 8:07 min (400 vol) scan at rest while subjects fixated on a central white cross-hair and 2) 12:19 min scan (610 vol) scan consisting of 4 min of the SST performance, followed by a short 12 s transition period when a slide announced an upcoming 8 min rest. BOLD volumes during first 7 s of each scan were not considered to allow for calibrations and MR signal reaching steady state magnetization. Therefore, BOLD data assessed consisted of two fMRI scans of 8:00 and 12:12 min respectively (Fig. 1A for overview of the sequence of acquisitions).

Two short (16 s) spin echo EPI scans (TR/TE = 1560/49.8 ms, five in A-P and five in P-A phase direction) with an imaging volume and voxel size identical to the GE-EPI were acquired immediately before each BOLD fMRI scan. These phase-reversed spin echo EPI scans provided field map for correcting EPI geometric distortion (Smith et al., 2004). This procedure was performed using FSL's topup/applytopup (Smith et al., 2004), which yielded improved signal localization across the whole brain, with the most notable improvements in frontal and temporal areas (Smith et al., 2004). At the start of the imaging session and preceding the spin echo EPI scans, subjects received a T1-weighted anatomical MRI with whole brain coverage using a 3D Magnetization Prepared Rapid Gradient Echo (MPRAGE) sequence (5:12 min long, 176 sagittal slices, 1.1 × 1.1 × 1.2 mm³ voxels, GRAPPA R = 2 acceleration) per the Alzheimer's Disease Neuroimaging Initiative (ADNI-2) imaging protocol.

2.5. Preprocessing

fMRI data were processed with an in-house developed pipeline based on Matlab and FSL using state-of-the-art guidelines (Amico et al., 2017; Power et al. 2012, 2014). These steps included: BOLD volume unwarping with *applytopup*, slice timing correction (*slicetimer*), realignment (*mcflirt*), normalization to mode 1000, demeaning and linear detrending (Matlab *detrend*), regression (Matlab *regress*) of 18 signals: 3 translations, 3 rotations, and 3 tissue-based regressors (mean signal of whole-brain, white matter (WM) and cerebrospinal fluid (CSF)), as well as 9 corresponding derivatives (backwards difference; Matlab). A scrubbing procedure censoring high head motion volumes was based on two metrics: Frame Displacement (FD, in mm), and DVARS (D referring to temporal derivative of BOLD time courses, VARS referring to root mean square variance over

voxels) from Power et al., (2014). Specifically, we used the standardized DVARS as proposed in Afyouni et al. (Afyouni and Nichols, 2018). We also used SD (standard deviation of the BOLD signal within brain voxels at every time-point). The FD and DVARS vectors (obtained with *fsl_motion_outliers*) were used to tag outlier BOLD volumes with FD > 0.3 mm and standardized DVARS > 1.7. The SD vector obtained with Matlab was used to tag outlier BOLD volumes higher than 75 percentile +1.5 of the interquartile range per FSL recommendation (Jenkinson et al., 2012). Note that there was no significant difference in the number of censored volumes between the two FHA groups ($p = 0.15$ for the first resting-only fMRI scan, $p = 0.35$ for the second, task-rest scan, two-tailed t-test).

A bandpass first-order Butterworth filter [0.009 Hz, 0.08 Hz] was applied to all BOLD time-series at the voxel level (Matlab *butter* and *filtfilt*). The first three principal components of the BOLD signal in the WM and CSF tissue were regressed out of the gray matter (GM) signal (Matlab, *pca* and *regress*) at the voxel level. A whole-brain data-driven functional parcellation based on 278 regions, as obtained by Shen et al., (2013), was projected into each subject's T1 space (FSL *flirt* 6dof, FSL *flirt* 12dof and finally FSL *fnirt*) and then into native EPI space of each subject. We also applied FSL boundary-based-registration (Greve and Fischl, 2009) to improve the registration of the structural masks and the parcellation to the functional volumes. For the subcortical nodes, we implemented striatal regions as defined by Mawlawi et al., (2001) and thalamic regions defined by Behrens et al., (2003). The thalamic regions were further consolidated from 7 to 4 per hemisphere (pre-motor, primary motor, and sensory input regions were combined, and occipital and temporal-projecting regions were combined). This procedure resulted in a total number of 286 brain regions.

We estimated individual functional connectivity matrices using Pearson's correlation coefficient between the averaged signals of all region pairs. The resulting individual FC matrices were comprised of 286 cortical and subcortical nodes. Finally, the resulting functional connectomes were ordered according to seven cortical resting state networks (RSNs) as proposed by Yeo et al., (2011) (see insert of Fig. 2B). For completeness, we added two more networks: one comprised of the subcortical and one of the cerebellar regions.

2.6. Connectivity independent component analysis (connICA) on family history of alcoholism (FHA) data

connICA is a novel data-driven methodology that applies independent
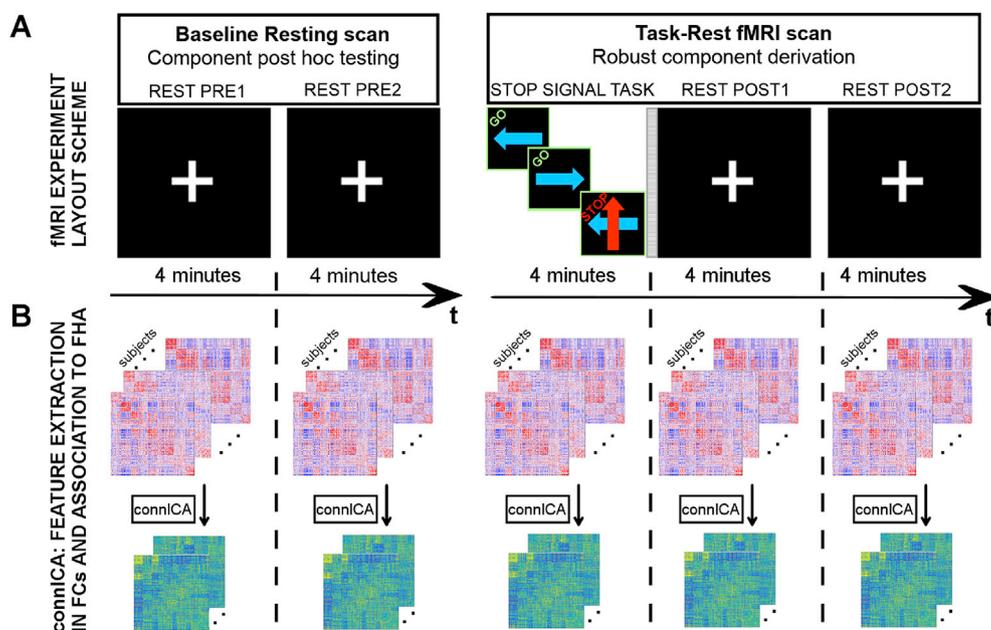
Fig. 1. Study design and functional connectivity (FC) analysis scheme. A) Each subject completed two fMRI scans: a baseline resting scan (*left*), with eyes fixated on a central white cross-hair; a task-rest fMRI scan (*right*) comprised a 4 min stop signal task (Logan and Cowan, 1984) in which the direction of a blue arrow prompted a left or right button press and a red arrow indicated the need to withhold the response to a blue arrow (labels on top of each tile are only illustrative and did not appear on the actual stimuli). Within this same scan the task was followed by a short 12 s intermission (indicated by a gray vertical stripe rectangle) when a slide announced the upcoming rest with the printed statement, "The task is over. Fix your gaze on the cross-hair for the remainder of the scan". Subjects then rested for 8 min and again fixated on a white central cross-hair. **B)** Both fMRI scans were subdivided into 4 min "static" segments (blocks), for which we independently estimated whole-brain functional connectomes and obtained independent connectivity components using the connICA method.
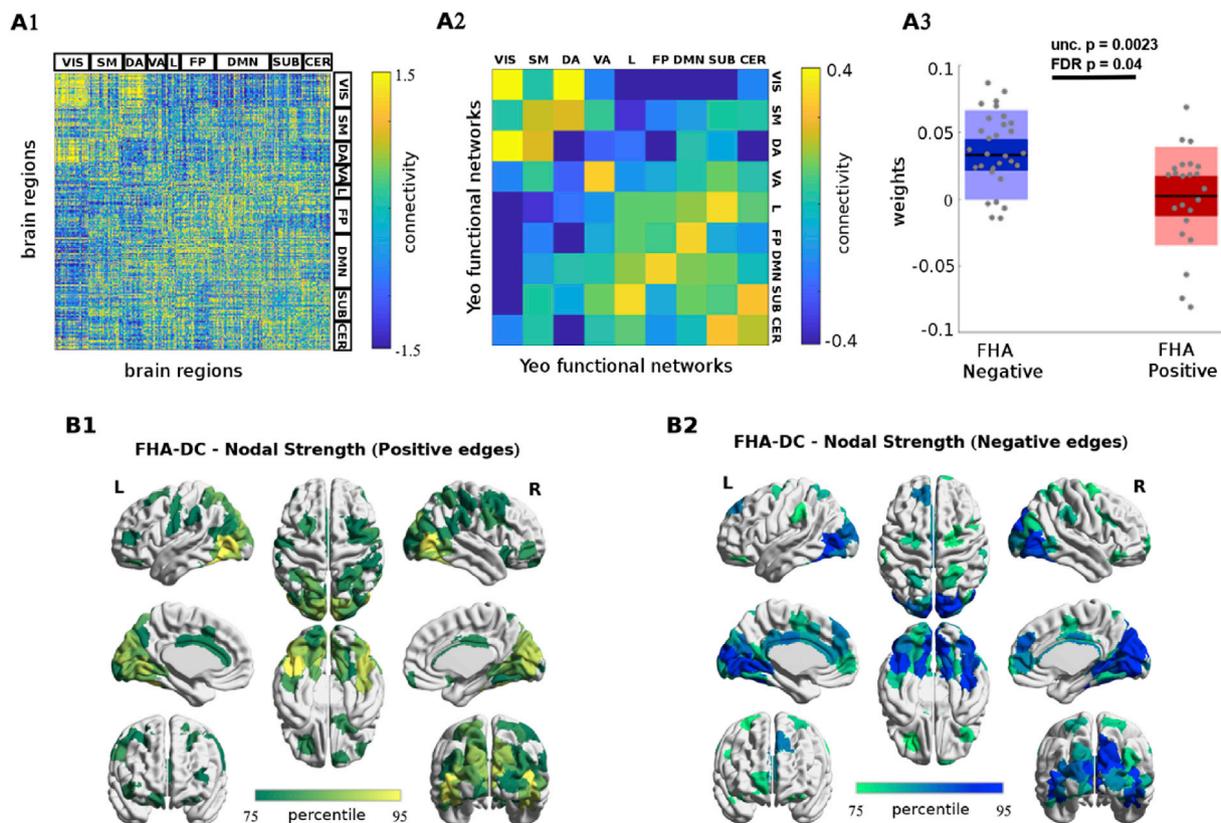
Fig. 2. Family history of alcoholism differentiating component (FHA-DC). A1) The functional connectivity reconfiguration component extracted by connICA in the REST POST1 window (i.e., within 4 min after completing the stop signal task). Pairwise associations between brain regions are ordered by resting-state functional networks as proposed by Yeo et al. (Yeo et al., 2011). **A2)** For clarity, the same component, depicted after averaging across functional networks, shows prominent connectivity between the visual and dorsal attention network areas, as well as between default-mode and frontoparietal networks. **A3)** Group differences in the individual subject weights associated with FHA-DC, two-tailed *t*-test between FHA negative and positive groups, $p = 0.0023$; False Discovery Rate (FDR, (Benjamini and Hochberg, 1995) adjusted p = 0.04, accounting for the 30 robust components)). **B1-B2)** Nodal strength (sum over columns of **A1,** including only: **B1)** positive edges or **B2)** negative edges) of the top 25% regions involved in the identified FHA-differentiating component.

component analysis (Amico et al., 2017) to extract independent connectivity patterns from individual functional connectomes. connICA's output includes: i) an "FC-component" representing an independent pattern of functional connectivity present across subjects, and ii) each subject's weight, quantifying the (signed) component strength or prominence in each individual FC matrix (see Fig. S1). connICA has been recently used in disentangling connectivity subsystems associated with levels of consciousness (Amico et al., 2017), Alzheimer's disease (Contreras et al., 2017), as well as in extracting "hybrid" connectivity features from sets of functional and structural connectomes (Amico and Goñi, 2018).

2.6.1. Static functional connectivity analyses

We divided both scans into 4-min periods (Fig. 1A), two during the baseline rest scan and three during the task-rest scans (TASK - first 4 min [omitting a 12 s slide instruction], REST POST1 - subsequent 4 min, and REST POST2 window - last 4 min). We then applied connICA separately in each 4-min block, testing for independent functional components or "components of interest" that significantly differentiated FHA (Fig. 1B). A component of interest must be (i) robust (appear in multiple ICA runs) and (ii) as per our hypothesis, associated with FHA during the task-rest fMRI scan (which includes SST, REST POST1 and REST POST 2 blocks; see Fig. 1). Given the non-deterministic nature of the ICA decomposition into components (Hyvarinen, 1999; Hyvärinen and Oja, 2000), multiple ICA runs are required to select the most robust outcomes (Amico et al., 2017; Hyvarinen, 1999). As in previous work, we accounted for this by evaluating the robustness of the components ("FC-traits" in (Amico et al., 2017)) over 100 FastICA runs. The FC-component was considered robust

when it appeared in at least 75% of the runs, as defined by a correlation of 0.75 or higher across runs (Amico et al., 2017).

Before running the connICA algorithm, we applied Principal Component Analysis (PCA (Jolliffe, 2014)) to perform noise filtering and dimensionality reduction, as recommended by work in machine learning (Särelä and Vigário, 2003) and neuroimaging communities (Calhoun et al., 2006; Kessler et al., 2014). After this PCA-based preprocessing, we estimated the number of independent components (Amico et al., 2017; Calhoun et al., 2009). The two parameters of percent retained variance from PCA and number of independent components were broadly explored to find the optimal combination. For each block, we examined percent variance retained after PCA in the range [75%, 100%], in steps of 5%. Similarly, we evaluated the number of ICA components in the range [5, 25], in steps of 5. An optimal choice was defined as *numRobustcomps (%) × numICAconvergence (%)*, i.e. where the number of robust components and the convergence of the fastICA algorithm across runs were both maximized (see Supplementary Fig. S2). As depicted in Fig. S2, the optimal choice of these two parameters was 85% retained variance in PCA and 15 independent components. Importantly, family history of alcohol or any other subject characteristic *was not* considered during this evaluation.

2.6.2. Anatomic similarities between a component of interest and an activation map for the [Stop > Go] BOLD contrast during the stop signal task

We evaluated the spatial overlap between a component of interest obtained through connICA and brain regions engaged by the stop signal task as follows: 1) The FC component of interest was summarized by the (positive) strength of brain regions by summing their positive

connectivity values, which were assigned a corresponding percentile rank based on their distribution. 2) We then created voxel-level nodal strength masks in one-percentile increments from the 50th to the 90th percentiles. 3) We assessed the overlap between the nodal strength mask and the activation map ([Stop > Go] contrast, $p < 0.05$ family-wise error (FWE), cluster-corrected using a $p = 0.001$ cluster forming threshold). 4) We computed the (i) percentage of voxels and (ii) the number of voxels within both the nodal strength mask and the activation mask. 5) We then developed a null model to assess overlap between the two masks that would be expected from chance distributions of the gray matter voxels. Specifically, for each percentile threshold assessed on the nodal strength map, the null distribution was created by randomly shuffling the voxels of the nodal strength mask in the gray matter 1000 times, while keeping the [Stop > Go] activation mask fixed.

2.6.3. Dynamic functional connectivity analyses

To refine the estimate of when any components of interest emerged, we employed a standard rectangular sliding window approach with four different window lengths (60, 75, 90 and 120 s, sliding in 6 s increments) and extracted dynamic functional connectomes (dFC) in each window. For every window we ran connICA using fixed parameters from the static case, specifically: 100 runs, 75% criterion for robust independent components, 85% PCA variance retained, 15 ICA components (see previous section for details). This same procedure was repeated 25 times in a *leave-two-out* fashion (one subject per group, one FHA negative and one FHA positive), to diminish the influence of possible outliers. For each identified component of interest, we proceeded as follows. For each sliding window (and for each leave-two-out run), the component of interest was correlated with the dynamic robust functional components found during both fMRI scans (i.e., both baseline rest and task-rest scans). The inclusion of both scans was needed to show that the component of interest was specific to the task-rest scan (i.e., not present during the baseline rest). To capture the dynamics of a component of interest along the course of the two fMRI scans, the best-matching dFC component (i.e. the one with the highest correlation in absolute value with the static component of interest) was reported within the sliding time window. Similarity between components was measured by a Pearson's correlation coefficient between the (vectorized) full connectivity profiles.

3. Results

3.1. FC component derivation

We employed an innovative data-driven independent component analysis of functional connectomes (connICA (Amico et al., 2017), also see Fig. S1) on fifty four subjects (23 with at least one first degree relative with alcoholism, 31 with no first or second degree relatives with alcoholism; see Table 1). In the "static" connICA step, we evaluated each of the five fMRI blocks (i.e. REST PRE1, REST PRE2, SST, REST POST1, REST POST2, each 4-minute long, see Fig. 1B and Methods for details). The aim was to search for a functional connectivity (FC) signature associated with family history of alcoholism (FHA) that we hypothesized would manifest solely during the post-task resting block. The procedure can be summarized as follows (see Methods section for details): 1) We first determined the optimal number of robust independent components, which turned out to be 15 for this dataset (see Fig. S2 caption for details). 2) Only those components that satisfied the robustness criterion were tested for associations with FHA. 3) The sole component found to be associated with FHA was then used in a sliding-window analysis to better characterize when it emerged and disappeared.

During the task-rest scan, connICA extracted 30 robust components: 12 during the SST, 11 during REST POST1 (see Figs. S4) and 7 during REST POST2. Among those, the static connICA data-driven analysis (Fig. 1B) resulted in a single component in REST POST1 that distinguished the FHA groups, as evident in group differences of the component weights. These weights were significantly lower in the FHA positive

subjects (two-tailed *t*-test, uncorrected p = 0.0023; false discovery rate (FDR, (Benjamini and Hochberg, 1995)) adjusted p = 0.04, accounting for the 30 robust components; Fig. 2A3), indicating that they had a diminished presence of this component.

The component emerged only during the 4 min rest following the task (i.e., REST POST1 block, Fig. 1) and was absent in the SST block and other three resting state blocks (i.e. REST PRE1, REST PRE2 and REST POST2). This FHA-Differentiating Component (FHA-DC) predominantly encompassed functional connectivity between the visual and dorsal attentional areas, and between associative visual areas and default-mode/fronto-parietal networks (Fig. 2A1-A2, Fig. 2B1-B2). Specifically, FHA-DC showed associative visual areas positively coupled with dorsal attentional cortices, as well as negatively coupled with default-mode/fronto-parietal networks (Fig. 2A1-A2, Fig. 2B1-B2). We repeated this analysis after excluding the three FHA positive subjects whose first degree relatives were mothers with alcoholism (i.e., despite subject reports to the contrary, to rule out any possible effect of significant fetal alcohol exposure). The FHA-DC remained present in the REST POST1 block (FHA-DC similarity with full (n = 54) sample of *r* = 0.9).

To assure that the FHA-DC component found through connICA was not dependent on the selected number of independent components (estimated to be 15 in this manuscript, see also Fig. S2), we tested for the presence of the FHA-DC across different numbers of derived components (from 11 to 20 in steps of 1; 100 realizations for each number of components evaluated). The component was identified (r > 0.95) for more than 80% of the realizations (see Fig. S3 for details).

3.2. FC component predictors

To better understand this functional reconfiguration component, we performed a multi-linear regression analysis to predict FHA-DC weights based on four FHA-related predictors. Specifically, FHA group membership, and three variables on which FHA groups differed: CESD scores measuring depressive symptoms, AUDIT scores reflecting alcohol use disorder symptoms, and recent self-reported drinking as assessed by grams of alcohol per week normalized by total body water to account for sex differences (Fig. 3A-B-C, also see Table 1). Four nuisance variables were also included to account for any potential effects of age, sex, head motion (number of scrubbed volumes, see Methods for details), and stop signal response time (SSRT, in milliseconds) to control for individual differences in motor inhibition during SST. In the multilinear model, sex was a significant effect ($p = 0.02$, Fig. 3A), while depression scores (CESD) showed trend-level significance ($p = 0.058$, Fig. 3A). Notably, after accounting for these factors, the between group difference in the FHA-DC was also a significant predictor of the multi-linear regression model ($p = 0.0011$, Fig. 3A). The linear relationship between the actual and predicted weights explains about 45% of the variance in the FHA-DC individual weights (Fig. 3B), with well-behaved residuals. Specifically, the residuals are symmetrically distributed, tending to cluster around 0, and within 2.5 standard deviations of zero (Fig. 3C).

3.3. Anatomic similarities between the FC component and stop signal task functional anatomy

To assess spatial overlap between brain regions active during SST (e.g., responses to Go and correct Stop trials; see Fig. 1A and Methods) and the FHA-DC subsystem observed during the transition to rest, we used trial-specific responses during SST (voxel-wise *t*-statistic maps, FWE cluster-corrected at $p < 0.05$, $p = 0.001$ cluster-forming threshold) and the top 25% most prominent brain "hubs" (in terms of positive nodal strength, Fig. 2B1) in FHA-DC. Specifically, the anatomic hubs of FHA-DC cover, on average, 18% ± 1% standard error (SE) of the Go trials' activation (Fig. 4B1, yellow bars); the Stop trials' activation coverage is 29% ± 1% SE (Fig. 4B2, yellow bars). Notably, the overlap is most extensive for the Stop compared to Go trials contrast (Fig. 4A3, also see (Kareken et al., 2013)). Particularly, the [Stop > Go] activation map coverage is
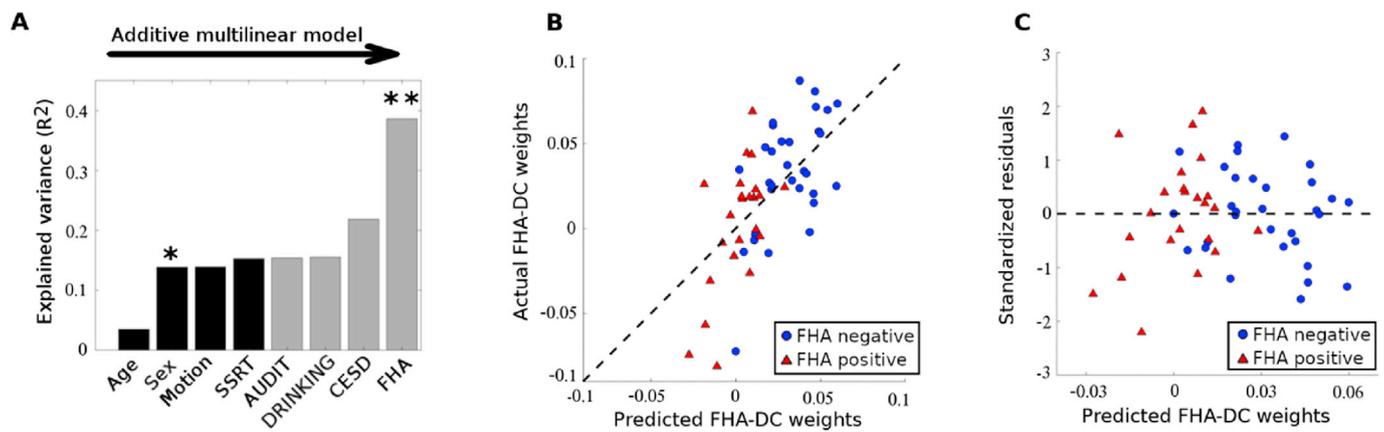
Fig. 3. FHA-DC individual weights predictability by family history of alcoholism, after accounting for possible confounds. A) Additive multi-linear regression model with predictors sequentially introduced in the order of: age, sex, head motion (number of scrubbed volumes), stop-signal response time (SSRT), AUDIT score, normalized drinking (see Methods), depression score (CESD), and FHA group membership. Significant predictors are indicated by one or two asterisks ($p < 0.05$ and $p < 0.01$, respectively). **B)** Scatter plot of the subject weights (average across connICA runs) associated with the extracted FHA-differentiating component versus the subject weights predicted by the final multi-linear regression model that includes all eight predictors in (A). Blue circles represent individual weights for the FHA negative group, red triangles represent individual weights for the FHA positive group. Dashed black line represents the identity line. **C)** Scatter plot of the standardized residuals versus the predicted subject weights associated with the FHA-DC for the multi-linear model shown in (A) (also see Methods for details).

43% ± 2% SE (Fig. 4B3, yellow bars). Furthermore, additional analyses spanning a wide range of nodal hub strengths (50th to 90th percentile rank) showed that the overlap between the FHA-DC and the [Stop > Go] activation map exceeded chance as defined by a spatial null model (see Fig. S5 and Methods for details on the null model).

Most importantly, the stop signal activation maps in each subject are computed in SPM12 during the SST block and derived using *a priori* general linear model-based analyses of the BOLD response modeled with a standard hemodynamic response function, completely independently of the connectivity analyses. Furthermore, the FH group effects assessed with independent two-sample *t*-tests in SPM12 showed no differences (peak voxel $p < 0.05$, family wise error (FWE)-corrected for multiple comparisons across the whole brain at a cluster-forming threshold of $p = 0.001$) in BOLD activation for each of the reported SST contrasts (Go, Stop, and Stop > Go). Also note that the applied thresholds for both SST activation and nodal strength connectivity maps emphasize the most prominent brain regions in both analyses, which lends an additional credence to the observed overlap between task activation and the anatomic distribution of the FHA-DC.

3.4. Dynamic connICA analysis

Of particular interest was the fact that, although the major hubs in the FHA-DC encompass brain circuitry that was strongly elicited by the SST, this component emerged only in the subsequent 4 min of rest (i.e., REST POST1). That is, the FHA-DC *did not manifest during the task,* but well after the task-induced hemodynamic response has decayed. To narrow the temporal dynamics of the FHA-DC in REST POST1, and determine if it was specific for that time period, we ran a post-hoc connICA analysis with a finer temporal resolution (2 min sliding window rather than "static" non-overlapping 4 min intervals) across both fMRI scans. Consistent with the static results, the FHA-DC was absent during the baseline rest (Fig. 5A), began only after task completion, and lasted transiently for approximately 3 min (Fig. 5B). These findings suggest that the connectivity component sensitive to differences in FHA occurred as subjects switched from the task itself *en route* to a state of quiet rest. We also explored shorter sliding windows and found the FHA-DC peak to be present, albeit less prominently, for 90 and 75 s window durations before fading at the 60 s window duration (Fig. S6). The temporal (i.e., onset and duration) and spatial (i.e., overlap with regions in a preceding task) characteristics of this component suggest its involvement in functional reconfiguration of the brain networks in the transition from cognitive effort to rest.

3.5. Relationship to impulsivity

Finally, we explored the extent to which behavioral impulsivity— a key feature of addiction risk (Amlung et al., 2017; Bickel et al., 2007)— related to the FHA-DC. Specifically, a subset of subjects ($n = 46$) had data available from a delay discounting paradigm, which quantifies subjects' devaluation of money as a function of delay to receipt. This "reward impatience" is a phenotype common to various addictions (Amlung et al., 2017; Bickel et al., 2007) and longitudinally predicts drug use (Fernie et al., 2013) and treatment outcomes (MacKillop and Kahler, 2009; Stanger et al., 2012). The area under the delay discounting curve (AUC) was significantly correlated with the FHA-DC weights ($r = 0.35$, $p = 0.018$; Fig. S8C), such that greater delayed reward preference ("patience") correlated with more of the FHA-DC trait. When entered into the additive multi-linear regression model, the FHA-DC remained significant; the AUC from the delay discounting curve remained significant, as well ($p = 0.034$; Fig. S8D).

4. Discussion

Alcoholism is highly prevalent (Grant et al., 2015) and few affected receive treatment (Cohen et al., 2007); after treatment, drinking relapse remains clinically significant (Anton et al., 2006; Schneekloth et al., 2012). Understanding brain-related vulnerabilities is thus important to prevention and public health, especially given alcoholism's comorbidity and joint risk with other mental illness (Walters et al., 2018).

Prior research of how FHA affects brain connectivity is not extensive, with past work using *a priori* seed regions (Cservenka et al., 2014) or seed-based analyses of data collected during cognitive tasks (Herting et al., 2011; Weiland et al., 2013; Wetherill et al., 2012). These data suggest that FHA may well affect reward and frontal circuit connectivity, as evident from related work (Cservenka, 2016). Broader analyses of whole brain regional network connectivity from resting state studies are less common, but also suggest altered frontal and dorsal premotor and sensorimotor connectivity between those with and without FHA (Holla et al., 2017; Vaidya et al., 2019).

We took a different approach. Rather than trying to distinguish between binary states of rest or cognitive task-related connectivity, we hypothesized that a transitional period between cognitive effort and rest might be more sensitive to FHA. Furthermore, we used a recently proposed, novel data-driven approach (Amico et al., 2017) to decompose whole-brain functional connectomes into independent components

driven by inter-subject variability (Fig. S1). This allowed us to isolate functional patterns sensitive to subject characteristics, or other behavioral or genetic variables— in the present case, the FHA-DC (Fig. 2, Fig. S4).

The result was a transient (approximate 3-minute long, Fig. 5) component of connectivity (Fig. 2) that emerged only after the task performance was completed. Those with FHA showed reduced presence of this functional brain reconfiguration, even after accounting for potential nuisance variables (age, sex, task performance, motion) and factors on which the FHA groups differed (depressive symptoms, recent drinking, drinking related problems; Fig. 3). Most importantly, had the analysis tested only for differences within the resting state scans (prior to the task, or in a separate resting state scan some minutes after task completion), or within the task period, this group difference would not have been detected.

Given the anatomic overlap with brain regions involved in the task (Fig. 4), the data also suggest that areas most active during the stop signal task (visual and attentional networks) remain mutually engaged several minutes after the task, with this functional coupling diminishing as subjects resume an introspective rest state (Fig. 5). This brain network reconfiguration process is less harmonized and significantly attenuated in FHA positive subjects (see weights in Fig. 2A3).

Other anatomic features of the FHA-DC included prominent within-network connectivity in the visual system, as well as negative connectivity between the visual network and ventral attention, limbic, frontoparietal, and default mode network areas. Recent studies using group ICA to identify functional connectivity networks find that in comparatively older individuals with more severe alcohol-related problems there is decreased functional connectivity in visual, sensory, and motor areas (Vergara et al. 2017, 2018). Similarly, machine learning can differentiate

alcohol use severity using connectivity features between sensorimotor, default mode, salience, and auditory networks (Fede et al., 2019). Insofar as FHA is a prominent risk for alcoholism, both these current data and findings from other whole brain connectivity studies (Holla et al., 2017; Vaidya et al., 2019) suggest that some of these network features may precede alcohol use.

To our knowledge, this is the first evidence that a brain-based endophenotype of FHA affects FC patterns in the dynamic transition from task engagement to rest. Elsewhere, however, the nature of networks' functional reconfiguration appears to play a prominent role in both cognitive shifts, as well as level of cognitive ability (Schultz and Cole, 2016; Shine et al. 2017, 2019; Shine and Poldrack, 2018). In this study, we present evidence that such a dynamic reconfiguration in the task-rest transition may be evident in familial risk for alcoholism.

Of particular note, a separate robust "resting-state network-like" (RSN-like) connectivity component (Fig. S4, Fig. S7) emerged across all fMRI blocks that was fundamentally distinct from the FHA-DC component. While this RSN-like component explained an expected large amount of variance (more than 20% of the variance in all blocks), it did *not* differentiate between FHA groups. This pervasive RSN-like component can then be viewed as the "resting-state core", as found in similar, recent studies (Amico et al., 2017; Cole et al. 2014; Contreras et al., 2017), co-occurring in parallel with many other independent connectivity processes (such as, in this case, the FHA-DC). This finding emphasizes the importance of connectivity decomposition to isolate other important processes from the predominant underlying connectivity pattern.

There are some technical considerations in understanding these data. This transitional connectivity reconfiguration was apparent using intermediate and longer sliding window durations (75–120 s, Fig. 5 and Fig. S6). This might be related to two main factors: the functional
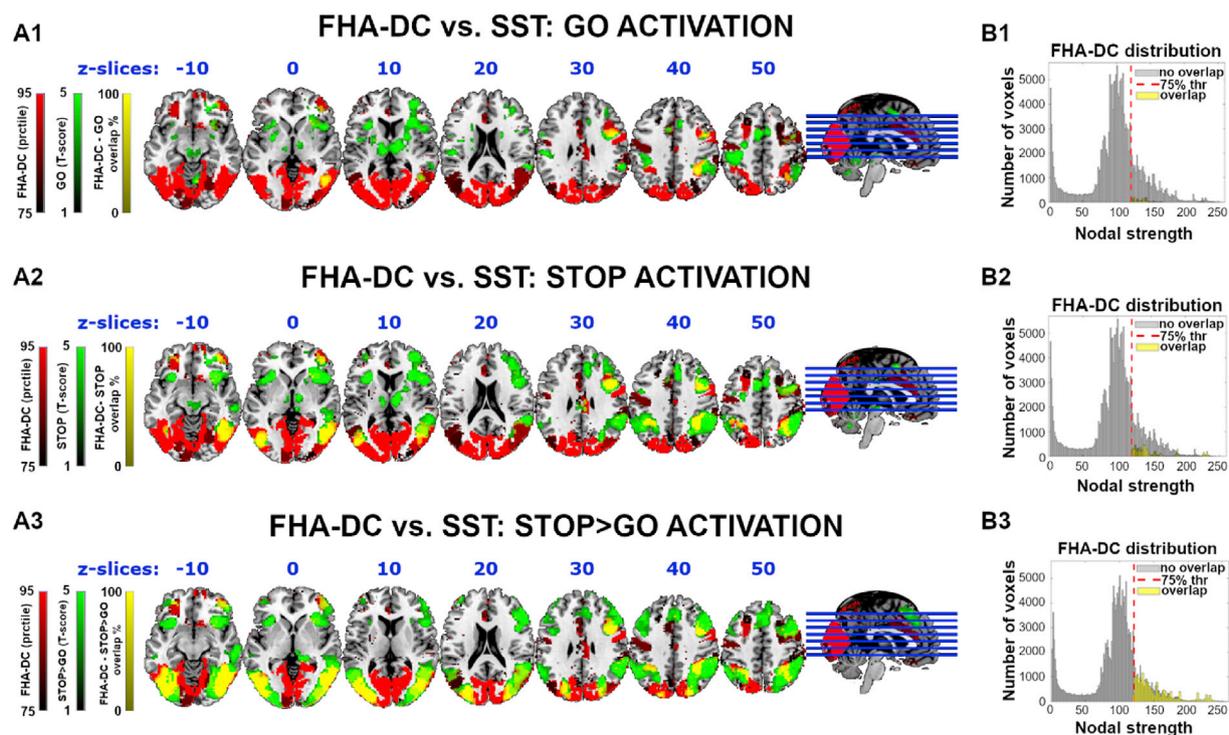
Fig. 4. Spatial overlap of brain regions engaged during stop signal task and top 25% nodal strength positive edges in the FHA-DC during REST-POST1 block. SST responding regions to **(A1)** successful GO trials, **(A2)** successfully inhibited Stop trials, **(A3)** the successful Stop > Go trials BOLD contrast (green overlay, t-statistic, voxel-wise FWE cluster-corrected at $p < 0.05$, $p = 0.001$ cluster-defining threshold). Red represents the most prominent regions (top 25% in nodal strength, including positive edges only) of the FHA-DC. The spatial overlap between BOLD activation and the anatomic distribution of the FHA-DC is most prominent in frontoparietal and lateral occipito-temporal regions (yellow overlay). **(B1-B3)** Histogram of the distribution of FHA-DC voxels that do (yellow bars), and do not (gray bars) overlap with the SST activation maps in (A1-A3). The [Stop > Go] contrast, which depicts highly engaged brain regions, overlaps the most and occurs along the right tails of the histogram, where the nodal strength of the FHA-differentiating component is greatest (red dashed lines indicate 75% nodal strength threshold; Thr). Axial slices ("z-slices" in the figure, in mm) indicate Montreal Neurological Institute (MNI) coordinate values.
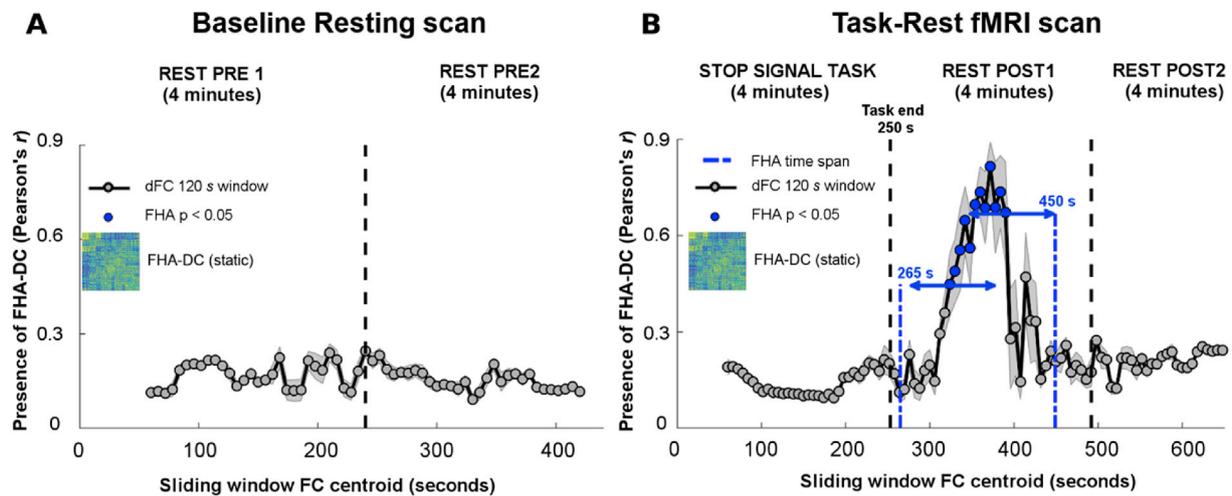
Fig. 5. Dynamics of the FHA-DC during both fMRI scans. 4A-4B). We ran connICA on each 120 s sliding window during the baseline resting scan **(A)** and task-rest fMRI scan **(B)**. The presence of the component (as reflected by Pearson's correlation coefficient, r) includes all subjects, regardless of the FHA status. The best matching correlation between the dynamic FC-component and the "static" FHA-DC (left inset, from Fig. 2A3) is shown across each sliding window centroid. Matching between components was measured by Pearson's correlation coefficient between the (vectorized) connectivity profiles. Vertical dashed lines indicate the separation between 4-minute "static" blocks (Figs. 1 and 2). Shaded gray bars indicate standard deviation across 25 bootstrap runs (see Methods for details). Blue dots indicate dynamic functional connectivity windows during which FHA groups significantly differ ($p < 0.05$), starting approximately 20 s after task cessation, and lasting for about 3 min, with an average peak correlation with the FHA-DC static result of 0.85 ± 0.15. Note the absence of significant correlations (on average 0.15 ± 0.05) between the originally extracted FHA-DC during REST POST1 and connectivity during the baseline resting scan as assessed using the sliding window.

reconfiguration process could have a characteristic time span (Telesford et al., 2016), and/or the functional connectivity data assessed here could possess noise characteristics that make it difficult to resolve the connectivity pattern at time windows shorter than 75 s (Hindriks et al., 2016). We also examined the dynamics using one particular brain parcellation scheme to define the elemental nodes for network analysis. Future studies will need to investigate these factors in more detail, with different task designs, and delve deeper into behavioral (cognitive, emotional) correlates of both the "after-task" reconfiguration, as well as transitional periods from rest to task.

Finally, the question remains as to what this transitional network reconfiguration process might precisely reflect. Two variables were significantly ($p < 0.05$) associated with the subjects' individual weights of the FHA-DC: biological sex (Fig. 3A), and delay discounting behavior ($n = 46$ sample, see Fig. S8); a third (depression scores) was significant at a trend level ($p < 0.06$). All three variables relate to alcoholism. Despite a recent narrowing in prevalence, alcoholism remains more common in men (White et al., 2015), who had a significantly smaller FHA-DC (Fig. S8). While both family history of alcoholism and delay discounting are potent risk factors and equally heritable (Anokhin et al., 2011; Kaprio et al., 1987; Nurnberger et al., 2004a), FHA positive subjects are not reliably more impulsive than FHA negative subjects (Petry et al., 2002). This suggests the possibility of a low-impulsivity protective factor, similar to high dopamine receptor availability (Volkow et al., 2006) in unaffected FHA positive, which may mediate this variability. FHA is also associated with risks for depression (Nurnberger et al., 2004b), with depression scores in this sample rising with less of the trait, mirroring the FHA pattern. Given the anatomic similarity between the stop signal task activation and the identified FHA-DC, it is also tempting to speculate that the transient network reorganization process could reflect an "attentional switch" that aids in returning the brain to an introspective-state. Future research will need to parse these potential associations and functions.

5. Conclusions

A functional connectivity pattern transiently emerged as subjects shifted from an active behavioral state to quiet rest. This functional subsystem is reduced in FHA positive subjects, and primarily involves visual, default-mode, and attentional networks, overlapping anatomically with structures active during the stop signal task. This novel finding suggests that brain endophenotypes of alcoholism (and potentially other kinds of behavioral disorders) may appear in brain network interactions while individuals transition away from external world engagement. The approach holds promise for understanding normal brain function, and more broadly, risk markers for psychiatric illness (Buckholtz and Meyer-Lindenberg, 2012).

Code availability

The connICA code (in MATLAB) used for this analysis is freely available at the CONNplexity Lab website: https://engineering.purdue.edu/ConnplexityLab/publications.

Author Contributions

Enrico Amico: Formal analysis, Writing – original draft, processed the MRI data, designed the framework and performed the connectivity analyses, interpreted the results, wrote the manuscript, Mario Dzemidzic: Conceptualization, Formal analysis, Writing – original draft, conceptualized and designed the fMRI study, collected and acquired the dataset, processed the MRI data, performed the stop signal task analysis, interpreted the results, wrote the manuscript, Brandon G. Oberlin: Formal analysis, Writing – original draft, programmed the delay discounting task and performed analyses, interpreted the results, wrote the manuscript, Claire R. Carron: Writing – original draft, collected and acquired the dataset, interpreted the results, wrote the manuscript, Jaroslaw Harezlak: Writing – original draft, interpreted the results, wrote the manuscript, Joaquín Goñi: Writing – original draft, Formal analysis, processed the MRI data, designed the framework and performed the connectivity analyses, interpreted the results, wrote the manuscript, David A. Kareken: Conceptualization, Writing – original draft, conceptualized and designed the fMRI study, interpreted the results, wrote the manuscript

Declaration of competing interest

The authors declare no competing financial interests.

Acknowledgments

Appendix A. Supplementary data

Supplementary data to this article can be found online at https://doi.org/10.1016/j.neuroimage.2020.116515.

References

Acheson, A., Tagamets, M.A., Rowland, L.M., Mathias, C.W., Wright, S.N., Hong, L.E., Kochunov, P., Dougherty, D.M., 2014. Increased forebrain activations in youths with family histories of alcohol and other substance use disorders performing a Go/NoGo task. Alcohol Clin. Exp. Res. 38 (12), 2944–2951.

Afyouni, S., Nichols, T.E., 2018. Insight and inference for DVARS. Neuroimage 172, 291–312.

Amico, E., Goñi, J., 2018. Mapping hybrid functional-structural connectivity traits in the human connectome. Netw. Neurosci. 2 (3), 306–322.

Amico, E., Marinazzo, D., Di Perri, C., Heine, L., Annen, J., Martial, C., Dzemidzic, M., Kirsch, M., Bonhomme, V., Laureys, S., et al., 2017. Mapping the functional connectome traits of levels of consciousness. Neuroimage 148, 201–211.

Amico, E., Arenas, A., Goñi, J., 2019. Centralized and distributed cognitive task processing in the human connectome. Netw. Neurosci. 3 (2), 455–474.

Amlung, M., Vedelago, L., Acker, J., Balodis, I., MacKillop, J., 2017. Steep delay discounting and addictive behavior: a meta-analysis of continuous associations. Addiction 112 (1), 51–62.

Anokhin, A.P., Golosheykin, S., Grant, J.D., Heath, A.C., 2011. Heritability of delay discounting in adolescence: a longitudinal twin study. Behav. Genet. 41 (2), 175–183.

Anton, R.F., O'Malley, S.S., Ciraulo, D.A., Cisler, R.A., Couper, D., Donovan, D.M., Gastfriend, D.R., Hosking, J.D., Johnson, B.A., LoCastro, J.S., et al., 2006. Combined pharmacotherapies and behavioral interventions for alcohol dependence: the combine study: a randomized controlled trial. J. Am. Med. Assoc. 295 (17), 2003–2017.

Band, G.P.H., van der Molen, M.W., Logan, G.D., 2003. Horse-race model simulations of the stop-signal procedure. Acta Psychol. 112 (2), 105–142.

Behrens, T.E.J., Johansen-Berg, H., Woolrich, M.W., Smith, S.M., Wheeler-Kingshott CaM, Boulby, P.A., Barker, G.J., Sillery, E.L., Sheehan, K., Ciccarelli, O., et al., 2003. Non-invasive mapping of connections between human thalamus and cortex using diffusion imaging. Nat. Neurosci. 6 (7), 750–757.

Benjamini, Y., Hochberg, Y., 1995. Controlling the false discovery rate - a practical and powerful approach to multiple testing. J. R. Stat. Ser. Soc. B Stat. Methodol. 57 (1), 289–300.

Bickel, W.K., Miller, M.L., Yi, R., Kowal, B.P., Lindquist, D.M., Pitcock, J.A., 2007. Behavioral and neuroeconomics of drug addiction: competing neural systems and temporal discounting processes. Drug Alcohol Depend. 90 (Suppl. 1), S85–S91.

Braun, U., Schafer, A., Walter, H., Erk, S., Romanczuk-Seiferth, N., Haddad, L., Schweiger, J.I., Grimm, O., Heinz, A., Tost, H., et al., 2015. Dynamic reconfiguration of frontal brain networks during executive cognition in humans. Proc. Natl. Acad. Sci. U. S. A. 112 (37), 11678–11683.

Bucholz, K.K., Cadoret, R., Cloninger, C.R., Dinwiddie, S.H., Hesselbrock, V.M., Nurnberger, J.I., Reich, T., Schmidt, I., Schuckit, M.A., 1994. A new, semi-structured psychiatric interview for use in genetic linkage studies: a report on the reliability of the SSAGA. J. Stud. Alcohol 55 (2), 149–158.

Buckholtz, J.W., Meyer-Lindenberg, A., 2012. Psychopathology and the human connectome: toward a transdiagnostic model of risk for mental illness. Neuron 74 (6), 990–1004.

Calhoun, V.D., Adali, T., Giuliani, N.R., Pekar, J.J., Kiehl, K.A., Pearlson, G.D., 2006. Method for multimodal analysis of independent source differences in schizophrenia: combining gray matter structural and auditory oddball functional data. Hum. Brain Mapp. 27 (1), 47–62.

Calhoun, V.D., Liu, J., Adalı, T., 2009. A review of group ICA for fMRI data and ICA for joint inference of imaging, genetic, and ERP data. Neuroimage 45 (1), S163–S172.

Chen, R.H., Ito, T., Kulkarni, K.R., Cole, M.W., 2018. The human brain traverses a common activation-pattern state space across task and rest. Brain Connect. 8 (7), 429–443.

Cohen, E., Feinn, R., Arias, A., Kranzler, H.R., 2007. Alcohol treatment utilization: findings from the national epidemiologic survey on alcohol and related conditions. Drug Alcohol Depend. 86 (2), 214–221.

Cole, Michael W., Bassett, Danielle S., Power, Jonathan D., Braver, Todd S., Petersen, Steven E., 2014. Intrinsic and task-evoked network architectures of the human brain. Neuron 83 (1), 238–251.

Colrain, I.M., 2015. Family history of alcoholism and brain activation: commentary on "Increased forebrain activations in youths with family histories of alcohol and other substance use disorders performing a Go/No-Go task. Alcohol Clin. Exp. Res. 39 (3), 403–404.

Contreras, J.A., Goñi, J., Risacher, S.L., Amico, E., Yoder, K., Dzemidzic, M., West, J.D., McDonald, B.C., Farlow, M.R., Sporns, O., et al., 2017. Cognitive complaints in older adults at risk for Alzheimer's disease are associated with altered resting-state networks. Alzheimer's Dementia: Diagn. Assess. Dis. Monit. 6, 40–49.

Cservenka, A., 2016. Neurobiological phenotypes associated with a family history of alcoholism. Drug Alcohol Depend. 158, 8–21.

Cservenka, A., Casimo, K., Fair, D.A., Nagel, B.J., 2014. Resting state functional connectivity of the nucleus accumbens in youth with a family history of alcoholism. Psychiatry Res. Neuroimaging 221 (3), 210–219.

Dougherty, D.M., Lake, S.L., Mathias, C.W., Ryan, S.R., Bray, B.C., Charles, N.E., Acheson, A., 2015. Behavioral impulsivity and risk-taking trajectories across early adolescence in youths with and without family histories of alcohol and other drug use disorders. Alcohol Clin. Exp. Res. 39 (8), 1501–1509.

Du, W., Green, L., Myerson, J., 2002. Cross-cultural comparisons of discounting delayed and probabilistic rewards. Psychol. Rec. 52 (4), 479–492.

Fede, S.J., Grodin, E.N., Dean, S.F., Diazgranados, N., Momenan, R., 2019. Resting state connectivity best predicts alcohol use severity in moderate to heavy alcohol users. Neuroimage Clin. 22, 101782.

Fernie, G., Peeters, M., Gullo, M.J., Christiansen, P., Cole, J.C., Sumnall, H., Field, M., 2013. Multiple behavioural impulsivity tasks predict prospective alcohol involvement in adolescents. Addiction 108 (11), 1916–1923.

Gallen, C.L., Turner, G.R., Adnan, A., D'Esposito, M., 2016. Reconfiguration of brain network architecture to support executive control in aging. Neurobiol. Aging 44, 42–52.

Gonzalez-Castillo, J., Bandettini, P.A., 2018. Task-based dynamic functional connectivity: recent findings and open questions. Neuroimage 180, 526–533.

Grant, B.F., Goldstein, R.B., Saha, T.D., Chou, S.P., Jung, J., Zhang, H., Pickering, R.P., Ruan, W.J., Smith, S.M., Huang, B., et al., 2015. Epidemiology of DSM-5 alcohol use disorder: results from the national epidemiologic survey on alcohol and related conditions III. JAMA Psychiatr. 72 (8), 757–766.

Greve, D.N., Fischl, B., 2009. Accurate and robust brain image alignment using boundary-based registration. Neuroimage 48 (1), 63–72.

Gustavson, D.E., Stallings, M.C., Corley, R.P., Miyake, A., Hewitt, J.K., Friedman, N.P., 2017. Executive functions and substance use: relations in late adolescence and early adulthood. J. Abnorm. Psychol. 126 (2), 257–270.

Hardee, J.E., Weiland, B.J., Nichols, T.E., Welsh, R.C., Soules, M.E., Steinberg, D.B., Zubieta, J.-K., Zucker, R.A., Heitzeg, M.M., 2014. Development of impulse control circuitry in children of alcoholics. Biol. Psychiatry 76 (9), 708–716.

Heiman, G.A., Ogburn, E., Gorroochurn, P., Keyes, K.M., Hasin, D., 2008. Evidence for a two-stage model of dependence using the NESARC and its implications for genetic association studies. Drug Alcohol Depend. 92 (1), 258–266.

Herting, M.M., Fair, D., Nagel, B.J., 2011. Altered fronto-cerebellar connectivity in alcohol-naïve youth with a family history of alcoholism. Neuroimage 54 (4), 2582–2589.

Hindriks, R., Adhikari, M.H., Murayama, Y., Ganzetti, M., Mantini, D., Logothetis, N.K., Deco, G., 2016. Can sliding-window correlations reveal dynamic functional connectivity in resting-state fMRI? Neuroimage 127, 242–256.

Holla, B., Panda, R., Venkatasubramanian, G., Biswal, B., Bharath, R.D., Benegal, V., 2017. Disrupted resting brain graph measures in individuals at high risk for alcoholism. Psychiatry Res. Neuroimaging 265, 54–64.

Hyvarinen, A., 1999. Fast and robust fixed-point algorithms for independent component analysis. IEEE Trans. Neural Netw. 10 (3), 626–634.

Hyvärinen, A., Oja, E., 2000. Independent component analysis: algorithms and applications. Neural Netw. 13 (4), 411–430.

Jenkinson, M., Beckmann, C.F., Behrens, T.E.J., Woolrich, M.W., Smith, S.M., 2012. FSL. NeuroImage 62 (2), 782–790.

Johnson, M.W., Bickel, W.K., 2008. An algorithm for identifying nonsystematic delay-discounting data. Exp. Clin. Psychopharmacol 16 (3), 264–274.

Jolliffe, I., 2014. Principal Component Analysis. Wiley StatsRef: Statistics Reference Online. John Wiley & Sons, Ltd.

Kaprio, J., Koskenvuo, M., Langinvainio, H., Romanov, K., Sarna, S., Rose, R.J., 1987. Genetic influences on use and abuse of alcohol: a study of 5638 adult Finnish twin brothers. Alcohol Clin. Exp. Res. 11 (4), 349–356.

Kareken, D.A., Dzemidzic, M., Wetherill, L., Eiler, W., Oberlin, B.G., Harezlak, J., Wang, Y., O'Connor, S.J., 2013. Family history of alcoholism interacts with alcohol to affect brain regions involved in behavioral inhibition. Psychopharmacology 228 (2), 335–345.

Kessler, D., Angstadt, M., Welsh, R.C., Sripada, C., 2014. Modality-spanning deficits in attention-deficit/hyperactivity disorder in functional networks, gray matter, and white matter. J. Neurosci. 34 (50), 16555–16566.

Lewis, C.M., Baldassarre, A., Committeri, G., Romani, G.L., Corbetta, M., 2009. Learning sculpts the spontaneous activity of the resting human brain. Proc. Natl. Acad. Sci. 106 (41), 17558–17563.

Logan, G.D., Cowan, W.B., 1984. On the ability to inhibit thought and action: a theory of an act of control. Psychol. Rev. 91 (3), 295–327.

MacKillop, J., Kahler, C.W., 2009. Delayed reward discounting predicts treatment response for heavy drinkers receiving smoking cessation treatment. Drug Alcohol Depend. 104 (3), 197–203.

Mawlawi, O., Martinez, D., Slifstein, M., Broft, A., Chatterjee, R., Hwang, D.-R., Huang, Y., Simpson, N., Ngo, K., Van Heertum, R., et al., 2001. Imaging human mesolimbic dopamine transmission with Positron emission tomography: I accuracy and precision of D2 receptor parameter measurements in ventral striatum. J. Cereb. Blood Flow Metab. 21 (9), 1034–1057.

Mennes, M., Kelly, C., Zuo, X.N., Di Martino, A., Biswal, B.B., Castellanos, F.X., Milham, M.P., 2010. Inter-individual differences in resting-state functional connectivity predict task-induced BOLD activity. Neuroimage 50 (4), 1690–1701.

Moss, H.B., Chen, C.M., Yi, H-y, 2007. Subtypes of alcohol dependence in a nationally representative sample. Drug Alcohol Depend. 91 (2), 149–158.

Nigg, J.T., Glass, J.M., Wong, M.M., Poon, E., Jester, J.M., Fitzgerald, H.E., Puttler, L.I., Adams, K.M., Zucker, R.A., 2004. Neuropsychological executive functioning in children at elevated risk for alcoholism: findings in early adolescence. J. Abnorm. Psychol. 113 (2), 302–314.

Nurnberger Jr., J.I., Wiegand, R., Bucholz, K., O'Connor, S., Meyer, E.T., Reich, T., Rice, J., Schuckit, M., King, L., Petti, T., et al., 2004a. A family study of alcohol dependence: coaggregation of multiple disorders in relatives of alcohol-dependent probands. Arch. Gen. Psychiatr. 61 (12), 1246–1256.

Nurnberger, J.I., Wiegand, R., Bucholz, K., O'Connor, S., Meyer, E.T., Reich, T., Rice, J., Schuckit, M., King, L., Petti, T., et al., 2004b. A family study of alcohol dependence: coaggregation of multiple disorders in relatives of alcohol-DependentProbands. Arch. Gen. Psychiatr. 61 (12), 1246–1256.

Petry, N.M., Kirby, K.N., Kranzler, H.R., 2002. Effects of gender and family history of alcohol dependence on a behavioral task of impulsivity in healthy subjects. J. Stud. Alcohol 63 (1), 83–90.

Porjesz, B., Rangaswamy, M., Kamarajan, C., Jones, K.A., Padmanabhapillai, A., Begleiter, H., 2005. The utility of neurophysiological markers in the study of alcoholism. Clin. Neurophysiol. 116 (5), 993–1018.

Power, J.D., Barnes, K.A., Snyder, A.Z., Schlaggar, B.L., Petersen, S.E., 2012. Spurious but systematic correlations in functional connectivity MRI networks arise from subject motion. Neuroimage 59 (3), 2142–2154.

Power, J.D., Mitra, A., Laumann, T.O., Snyder, A.Z., Schlaggar, B.L., Petersen, S.E., 2014. Methods to detect, characterize, and remove motion artifact in resting state fMRI. Neuroimage 84, 320–341.

Pyka, M., Beckmann, C.F., Schöning, S., Hauke, S., Heider, D., Kugel, H., Arolt, V., Konrad, C., 2009. Impact of working memory load on fMRI resting state pattern in subsequent resting phases. PLoS One 4 (9), e7198.

Raichle, M.E., MacLeod, A.M., Snyder, A.Z., Powers, W.J., Gusnard, D.A., Shulman, G.L., 2001. A default mode of brain function. Proc. Natl. Acad. Sci. 98 (2), 676–682.

Särelä, J., Vigário, R., 2003. Overlearning in marginal distribution-based ICA: analysis and solutions. J. Mach. Learn. Res. 4 (Dec), 1447–1469.

Schneekloth, T.D., Biernacka, J.M., Hall-Flavin, D.K., Karpyak, V.M., Frye, M.A., Loukianova, L.L., Stevens, S.R., Drews, M.S., Geske, J.R., Mrazek, D.A., 2012. Alcohol craving as a predictor of relapse. Am. J. Addict. 21 (s1), S20–S26.

Schultz, D.H., Cole, M.W., 2016. Higher intelligence is associated with less task-related brain network reconfiguration. J. Neurosci. 36 (33), 8551–8561.

Shen, X., Tokoglu, F., Papademetris, X., Constable, R.T., 2013. Groupwise whole-brain parcellation from resting-state fMRI data for network node identification. Neuroimage 82, 403–415.

Shine, J.M., Poldrack, R.A., 2018. Principles of dynamic network reconfiguration across diverse brain states. Neuroimage 180, 396–405.

Shine, J.M., Kucyi, A., Foster, B.L., Bickel, S., Wang, D., Liu, H., Poldrack, R.A., Hsieh, L.-T., Hsiang, J.C., Parvizi, J., 2017. Distinct patterns of temporal and directional connectivity among intrinsic networks in the human brain. J. Neurosci. 37 (40), 9667–9674.

Shine, J.M., Breakspear, M., Bell, P.T., Martens, K.A.E., Shine, R., Koyejo, O., Sporns, O., Poldrack, R.A., 2019. Human cognition involves the dynamic integration of neural activity and neuromodulatory systems. Nat. Neurosci. 22 (2), 289.

Shulman, G.L., Corbetta, M., Buckner, R.L., Fiez, J.A., Miezin, F.M., Raichle, M.E., Petersen, S.E., 1997. Common blood flow changes across visual tasks: I. Increases in subcortical structures and cerebellum but not in nonvisual cortex. J. Cogn. Neurosci. 9 (5), 624–647.

Smith, S.M., Jenkinson, M., Woolrich, M.W., Beckmann, C.F., Behrens, T.E.J., Johansen-Berg, H., Bannister, P.R., De Luca, M., Drobnjak, I., Flitney, D.E., et al., 2004. Advances in functional and structural MR image analysis and implementation as FSL. Neuroimage 23, S208–S219.

Stanger, C., Ryan, S.R., Fu, H., Landes, R.D., Jones, B.A., Bickel, W.K., Budney, A.J., 2012. Delay discounting predicts adolescent substance abuse treatment outcome. Exp. Clin. Psychopharmacol 20 (3), 205–212.

Telesford, Q.K., Lynall, M.-E., Vettel, J., Miller, M.B., Grafton, S.T., Bassett, D.S., 2016. Detection of functional brain network reconfiguration during task-driven cognitive states. Neuroimage 142, 198–210.

Vaidya, J.G., Elmore, A.L., Wallace, A., Langbehn, D.R., Kramer, J.R., Kuperman, S., O'Leary, D.S., 2019. Association between age and familial risk for alcoholism on functional connectivity in adolescence. J. Am. Acad. Child Adolesc. Psychiatry 58 (7), 692–701.

Vergara, V.M., Liu, J., Claus, E.D., Hutchison, K., Calhoun, V., 2017. Alterations of resting state functional network connectivity in the brain of nicotine and alcohol users. Neuroimage 151, 45–54.

Vergara, V.M., Weiland, B.J., Hutchison, K.E., Calhoun, V.D., 2018. The impact of combinations of alcohol, nicotine, and cannabis on dynamic brain connectivity. Neuropsychopharmacology 43 (4), 877–890.

Volkow, N.D., Wang, G.J., Begleiter, H., Porjesz, B., Fowler, J.S., Telang, F., Wong, C., Ma, Y., Logan, J., Goldstein, R., et al., 2006. High levels of dopamine D2 receptors in unaffected members of alcoholic families: possible protective factors. Arch. Gen. Psychiatr. 63 (9), 999–1008.

Walters, R.K., Polimanti, R., Johnson, E.C., McClintick, J.N., Adams, M.J., Adkins, A.E., Aliev, F., Bacanu, S.-A., Batzler, A., Bertelsen, S., et al., 2018. Transancestral GWAS of alcohol dependence reveals common genetic underpinnings with psychiatric disorders. Nat. Neurosci. 21 (12), 1656.

Weiland, B.J., Welsh, R.C., Yau, W.-Y.W., Zucker, R.A., Zubieta, J.-K., Heitzeg, M.M., 2013. Accumbens functional connectivity during reward mediates sensation-seeking and alcohol use in high-risk youth. Drug Alcohol Depend. 128 (1), 130–139.

Wetherill, R.R., Bava, S., Thompson, W.K., Boucquey, V., Pulido, C., Yang, T.T., Tapert, S.F., 2012. Frontoparietal connectivity in substance-naïve youth with and without a family history of alcoholism. Brain Res. 1432, 66–73.

Whelan, R., Watts, R., Orr, C.A., Althoff, R.R., Artiges, E., Banaschewski, T., Barker, G.J., Bokde, A.L.W., Büchel, C., Carvalho, F.M., et al., 2014. Neuropsychosocial profiles of current and future adolescent alcohol misusers. Nature 512 (7513), 185–189.

White, A., Castle, I.J.P., Chen, C.M., Shirley, M., Roach, D., Hingson, R., 2015. Converging patterns of alcohol use and related outcomes among females and males in the United States, 2002 to 2012. Alcohol Clin. Exp. Res. 39 (9), 1712–1726.

Xu, J., Moeller, S., Auerbach, E.J., Strupp, J., Smith, S.M., Feinberg, D.A., Yacoub, E., Uğurbil, K., 2013. Evaluation of slice accelerations using multiband echo planar imaging at 3T. Neuroimage 83, 991–1001.

Yeo, T.B.T., Krienen, F.M., Sepulcre, J., Sabuncu, M.R., Lashkari, D., Hollinshead, M., Roffman, J.L., Smoller, J.W., Zöllei, L., Polimeni, J.R., et al., 2011. The organization of the human cerebral cortex estimated by intrinsic functional connectivity. J. Neurophysiol. 106 (3), 1125–1165.

Young, S.E., Friedman, N.P., Miyake, A., Willcutt, E.G., Corley, R.P., Haberstick, B.C., Hewitt, J.K., 2009. Behavioral disinhibition: liability for externalizing spectrum disorders and its genetic and environmental relation to response inhibition across adolescence. J. Abnorm. Psychol. 118 (1), 117–130.